Development of Holistic Three-Dimensional Models for Cold Spray Supersonic Jet

S.H. Zahiri, T.D. Phan, S.H. Masood, and M. Jahedi

A three-dimensional, computational fluid dynamics (CFD) model is developed to estimate cold spray gas conditions. This model is calibrated and validated with respect to thermal history of a substrate exposed to the cold spray supersonic jet. The proposed holistic model is important to track state of gas and particles from injection point to the substrate surface with significant benefits for optimization of very rapid "nanoseconds" cold spray deposition. The three-dimensional model is developed with careful attention with respect to computation time to benefit broader cold spray industry with limited access to supercomputers. The k-ε-type CFD model is evaluated using measured temperature for a titanium substrate exposed to cold spray nitrogen at 800 °C and 3 MPa. The model important parameters are detailed including domain meshing method with turbulence, and dissipation coefficients during spraying. Heat transfer and radiation are considered for the de Laval nozzle used in experiments. The calibrated holistic model successfully estimated state of the gas for chosen high temperature and high pressure cold spray parameters used in this study. Further to this, the holistic model predictions with respect to the substrate maximum temperature had a good agreement with earlier findings in the literature.

1. Introduction

Cold spray process is a solid-state additive manufacturing technology that offers a cost-effective and energy efficient alternative for many coating and direct fabrication processes. In this technology, powder in a carrier gas is accelerated under high pressure and temperature using a De Laval-type nozzle to well above supersonic velocities (~500-1500 m/s) (Ref 1–6). The impact of particles to substrate in solid state results in a unique bond formation in nanoseconds that allows for the development of novel coatings, additive manufacturing of bulk materials, and prototyping.

Utilization of cold spray at high temperature and pressure (i.e., 800 °C and 3 MPa) imposes considerable limitations in experimental characterization and evaluation of supersonic jet conditions (i.e., temperature, pressure, and velocity) that are paramount for successful optimization of deposition process. Such experimentation is generally extremely difficult without disruption of supersonic gas flow from its original state. An example of such limitation is the ability to experimentally evaluate

Nomenclature

c	Local speed of sound in fluid (m/s)
c_p	Specific heat capacity at constant pressure (m²/s² K)
$C_{\varepsilon 1}$	k-ε turbulence model constant
$C_{\varepsilon 2}$	k-ε turbulence model constant
C_μ	k-ε turbulence model constant
C_{Clip}	Clip factor coefficient for turbulence energy
C_{Scale}	Scaling coefficient for curvature correction
g	Gravity vector (m/s²)
h	Specific static (thermodynamic) enthalpy (m²/s²)
h_{tot}	Specific total enthalpy (m²/s²)
k	Turbulent kinetic energy per unit mass (m²/s²)
M	Local Mach number, U/c (Dimensionless)
p'	Modified pressure (kg/m s²)
p	Static (thermodynamic) pressure (kg/m s²)
P_k	Turbulence energy (kg/m s³)
p_{ref}	Reference pressure (kg/m s²)
Pr_t	Turbulent Prandtl Number, $c_p \, \mu_t/\lambda_t$ (Dimensionless)
p_{tot}	Total pressure (kg/m s²)
R_0	Universal gas constant = 8.3145 (m³ Pa /K mol)
Re	Reynolds number (Dimensionless)
Sc_t	Turbulent Schmidt Number, μ_t/Γ_t (Dimensionless)
s_{strnr}	Shear strain rate (1/s)
t	Time (s)
T_{dom}	Domain temperature (K)
T_{stat}	Static (thermodynamic) temperature (K)
T_{tot}	Total temperature (K)
U	Velocity magnitude (m/s)
u	Fluctuating velocity component (m/s)
ε	Turbulent (Eddy) dissipation rate (m²/s³)

S.H. Zahiri and **M. Jahedi**, CSIRO Materials Science and Engineering, Gate 5, Normanby Road, Clayton, VIC 3168, Australia; and **T.D. Phan** and **S.H. Masood**, Swinburne University of Technology, 545 Burwood Road, Hawthorn, VIC 3122, Australia. Contact e-mail: saden.zahiri@csiro.au.

κ	Von Karman constant (0.41)
λ	Thermal conductivity (kg/m s^3 K)
μ	Molecular (dynamic) viscosity (kg/m s)
μ_{eff}	Effective viscosity, $\mu + \mu_{\mathrm{t}}$ (kg/m s)
μ_{t}	Turbulent (Eddy) viscosity (kg/m s)
ρ	Density (kg/m^3)
σ_{k}	k-ε turbulence model constant (1)
σ_{ε}	k-ε turbulence model constant (1.3)
Γ_{t}	Turbulent diffusivity (kg/m s)
θ	Nondimensionalized temperature
T_{g}	Cold spray stagnation temperature (ºC)
T_{w}	Measured substrate temperature (ºC)

state of individual cold spray particles (i.e., temperature and shock load pressure) through the deposition process.

Earlier studies by Fukumoto et al. (Ref 7), Wong et al. (Ref 8) and Legoux et al. (Ref 9) have demonstrated the effect of cold spray jet and substrate temperature on deposition efficiency and particle-substrate bond formation. In a recent study Li et al. (Ref 10) developed a two-dimensional (2D) model to investigate temperature distribution within cold spray nozzle wall and substrate with limited information on the events that occur between nozzle exit and substrate. Similarly, Yin et al. (Ref 11) evaluated a 2D model to examine substrate preheating for cold spray jet without consideration of the heat transfer between the gas and nozzle body. Wilcox (Ref 12) has reported that current 2D axisymmetric models (Ref 13) could introduce large errors particularly when k-ε-type turbulence model used for round jet.

Ryabinin et al. 2012 (Ref 14) determined Nusselt numbers of the impinging cold spray jet at relatively low cold spray gas temperature 100-200 °C and pressure 0.69 MPa. A similar approach by Lee et al. (Ref 15) led to experimental determination of the Nusselt number for a quasi-one-dimensional model that estimated supersonic jet conditions impinging onto an inclined (45°) flat plate. Ramanujachari et al. (Ref 16) and Belov et al. (Ref 17) investigated heat flux generated from a supersonic jet impinging onto a substrate to estimate Nusselt number. Rahimi et al. (Ref 18) measured substrate temperature when unheated air supersonic jet impinged onto a stainless steel foil. In this study, complicated nature of the jet-substrate interaction was revealed particularly when substrate distance from nozzle exit was three times the nozzle diameter. Other CFD models for extreme conditions of cold spray process have been published with limited experimental evaluation of the cold spray supersonic jet (Ref 12, 13, 19–22).

A common focus of the above studies is consideration of certain sections of the cold spray system (i.e., substrate, nozzle, deposited material, etc). Such approach, however, overlooks interconnected nature of the cold spray system. For example, generally the length scale near the wall, substrate, is affected by length scales of the jet turbulence retaining a memory of the upstream. Knowing this, it seems that a more realistic approach is to develop a holistic model for cold spray that estimates state of the gas and particles from injection point to the deposition zone. This study aims to model the whole field of the cold spray

gas stream in that the CFD model retains spatial connectivity for instant tracking of individual particles through the whole flow field.

To develop the holistic 3D model, a broadly used k-ε-type CFD model was calibrated for cold spray jet impinging onto a titanium substrate at 550 °C and 1.4 MPa. The calibration was accomplished with respect to turbulence coefficient, dissipation coefficient, and gas Prandtl number. Initial and boundary conditions were defined and the effects of various important parameters were considered. Finally, the calibrated model was successfully evaluated for cold spray experimental conditions of 800 °C and 3 MPa with approximately 11% average error. The estimated maximum temperature of substrate had a good agreement with results in literature.

2. Numerical Analysis

The CFD numerical simulations were based on Reynolds-Average Navier-Stokes (RANS)-type equations which generally require significant computational time (days) for complicated cold spray supersonic jet formation. Here, RANS is adopted to develop the model with considerably shorter computational time (hours) and consideration of fundamentals for supersonic jet. The proposed model is aimed to benefit broader cold spray industry to adopt and utilize the CFD model with computational power of current advanced personal computers as opposed to supercomputers. To enable the effects of turbulence to be predicted with less computational effort, several CFD researchers (Ref 23–27) have developed methods which modify the original unsteady Navier-Stokes equations by the introduction of averaged and fluctuating quantities to produce the new RANS equations.

2.1 Turbulence and Transport Equations

A widely used k-ε turbulence model (Ref 24) was used because it offers a good compromise between numerical effort and computational accuracy. This type of model was chosen due to its many advantages for development of robust yet practical models for industrial applications. The turbulence model has two main equations, which are the continuity and the momentum equation:

$$\frac{\partial \rho}{\partial t} + \frac{\partial}{\partial x_{\mathrm{j}}}\left(\rho U_{\mathrm{j}}\right) = 0, \qquad (\text{Eq } 1)$$

$$\frac{\partial \rho U_{\mathrm{i}}}{\partial t} + \frac{\partial}{\partial x_{\mathrm{j}}}\left(\rho U_{\mathrm{i}} U_{\mathrm{j}}\right) = -\frac{\partial p'}{\partial x_{\mathrm{i}}} + \frac{\partial}{\partial x_{\mathrm{j}}}\left[\mu_{\mathrm{eff}}\left(\frac{\partial U_{\mathrm{i}}}{\partial x_{\mathrm{j}}} + \frac{\partial U_{\mathrm{j}}}{\partial x_{\mathrm{i}}}\right)\right], \qquad (\text{Eq } 2)$$

where p' is the modified pressure which includes an additional term due to the turbulent normal stress, and the effective viscosity μ_{eff} accounting for turbulence in the model:

$$p' = p + \frac{2}{3}\rho k, \tag{Eq 3}$$

$$\mu_{\text{eff}} = \mu + \mu_t, \tag{Eq 4}$$

where μ_t is the turbulence viscosity. The k-ε model assumes that the turbulence viscosity is linked to the turbulence kinetic energy and dissipation via the relation:

$$\mu_t = C_\mu \rho \frac{k^2}{\varepsilon}, \tag{Eq 5}$$

whereas, turbulent kinetic energy k, which is defined as the variance of the fluctuations in velocity and the dissipation rate ε, the rate at which the velocity fluctuations dissipate, are obtained directly from the following differential transport equations.

$$\frac{\partial(\rho k)}{\partial t} + \frac{\partial}{\partial x_j}(\rho U_j k) = \frac{\partial}{\partial x_j}\left[\left(\mu + \frac{\mu_t}{\sigma_k}\right)\frac{\partial k}{\partial x_j}\right] + P_k - \rho\varepsilon, \tag{Eq 6}$$

$$\begin{aligned}\frac{\partial(\rho\varepsilon)}{\partial t} + \frac{\partial}{\partial x_j}(\rho U_j \varepsilon) &= \frac{\partial}{\partial x_j}\left[\left(\mu + \frac{\mu_t}{\sigma_\varepsilon}\right)\frac{\partial\varepsilon}{\partial x_j}\right] \\ &+ \frac{\varepsilon}{k}(C_{\varepsilon1}P_k - C_{\varepsilon2}\rho\varepsilon),\end{aligned} \tag{Eq 7}$$

where k and ε dimensions are (m^2/s^2) and (m^2/s^3), respectively. C_μ, $C_{\varepsilon1}$, $C_{\varepsilon2}$, σ_k, and σ_ε are turbulence constants depending on application and simulation conditions. Turbulent constants $C_{\varepsilon1}$ and $C_{\varepsilon2}$ due to their direct effect on turbulence production, and turbulence eddy dissipation were utilized for calibration of the model for supersonic jet. P_k is the turbulence production due to viscous forces, which is modeled using

$$P_k = \mu_t\left(\frac{\partial U_i}{\partial x_j} + \frac{\partial U_j}{\partial x_i}\right)\frac{\partial U_i}{\partial x_j} - \frac{2}{3}\frac{\partial U_k}{\partial x_k}\left(3\mu_t\frac{\partial U_k}{\partial x_k} + \rho k\right). \tag{Eq 8}$$

For compressible flow, $\frac{\partial U_k}{\partial x_k}$ is only large in regions with high velocity divergences, such as at a shock region (Ref 25).

2.2 Heat Transfer Equations

The total energy model and the ideal gas equation of state with temperature dependent material properties ($c_p(T)$, $\lambda(T)$, $\mu(T)$…), (Ref 12, 25) is used.

Firstly, the total enthalpy h_{tot} is directly computed from the Reynolds averaged total energy equation:

$$\begin{aligned}\frac{\partial \rho h_{\text{tot}}}{\partial t} - \frac{\partial p}{\partial t} + \frac{\partial}{\partial x_j}(\rho U_j h_{\text{tot}}) &= \frac{\partial}{\partial x_j}\left(\lambda\frac{\partial T}{\partial x_j} + \frac{\mu_t}{Pr_t}\frac{\partial h}{\partial x_j}\right) \\ &+ \frac{\partial}{\partial x_j}\left[U_i(\tau_{ij} - \rho\overline{u_i u_j})\right],\end{aligned} \tag{Eq 9}$$

where Pr_t is the turbulent Prandtl number. Static enthalpy h_{stat} which is a measure of the energy contained in a fluid per unit mass is derived from the relation:

$$h_{\text{tot}} = h_{\text{stat}} + \frac{1}{2}(U_i \cdot U_i) + k, \tag{Eq 10}$$

where U is the flow velocity with static temperature calculated using static enthalpy out of the relationship:

$$h_{\text{stat}} - h_{\text{ref}} = \int_{T_{\text{ref}}}^{T_{\text{stat}}} c_p(T)dT, \tag{Eq 11}$$

where $c_p(T)$ is specific heat at constant pressure. The default reference state is $T_{\text{ref}} = 0[K]$ and $h_{\text{ref}} = 0(\text{J/kg})$. Within solid domains, the conservation of energy equation can account for heat transport due to conduction.

$$\frac{\partial(\rho h)}{\partial t} = \nabla \cdot (\lambda\nabla T), \tag{Eq 12}$$

where h, ρ, and λ are the enthalpy, density, and thermal conductivity of the solid, respectively.

The ANSYS™ CFX Solver®, general grid interface (GGI), was utilized to allow heat transfer across the interface. At the GGI interface the gas-side and the solid-side temperatures were calculated based on heat flux conservation.

2.3 Computational Domain and Boundary Conditions

ANSYS™ CFX Solver® v14.0 was used to solve the numerical model. The CFD simulations computational grid in the present study is shown in Fig. 1a. The substrate was modeled as a $70 \times 70 \times 5$ mm^3 square flat plate, and the surface was assumed to have zero roughness. This assumption was due to smooth surface of the specimen and to adopt a less complicated approach to establish the early developments for holistic model of this study.

The surrounding domain was created as a cylinder with 400 mm diameter and 361.5 mm length. This domain consisted of three surfaces: a vertical face at nozzle pre-chamber section, a vertical face behind the substrate, and the main peripheral surface as shown in Fig. 1b with nitrogen as surrounding gas. It is worth noting that nitrogen was chosen as surrounding gas to avoid complexity and this assumption that large flow of the nitrogen through the cold spray nozzle provides high concentration of nitrogen in the imminent surrounding air which has already contained ~70% nitrogen as part of air composition.

A total pressure p_{tot} was specified as an inlet, nozzle entry, boundary condition at the pre-chamber plane of high pressure gas domain, Fig. 1c, and the direction was considered to be normal to the boundary. The total pressure was considered as the pressure that would exist at a point if the fluid was brought instantaneously to rest such that the dynamic energy of the flow converted to pressure without loss (Ref 28, 29). As the length scale near the wall is affected by length scales of the jet turbulence retaining a memory of the upstream, the whole field of the gas flow stream was modeled and calibrated, starting from the stable pressured stagnation section to the room pressured domain far field.
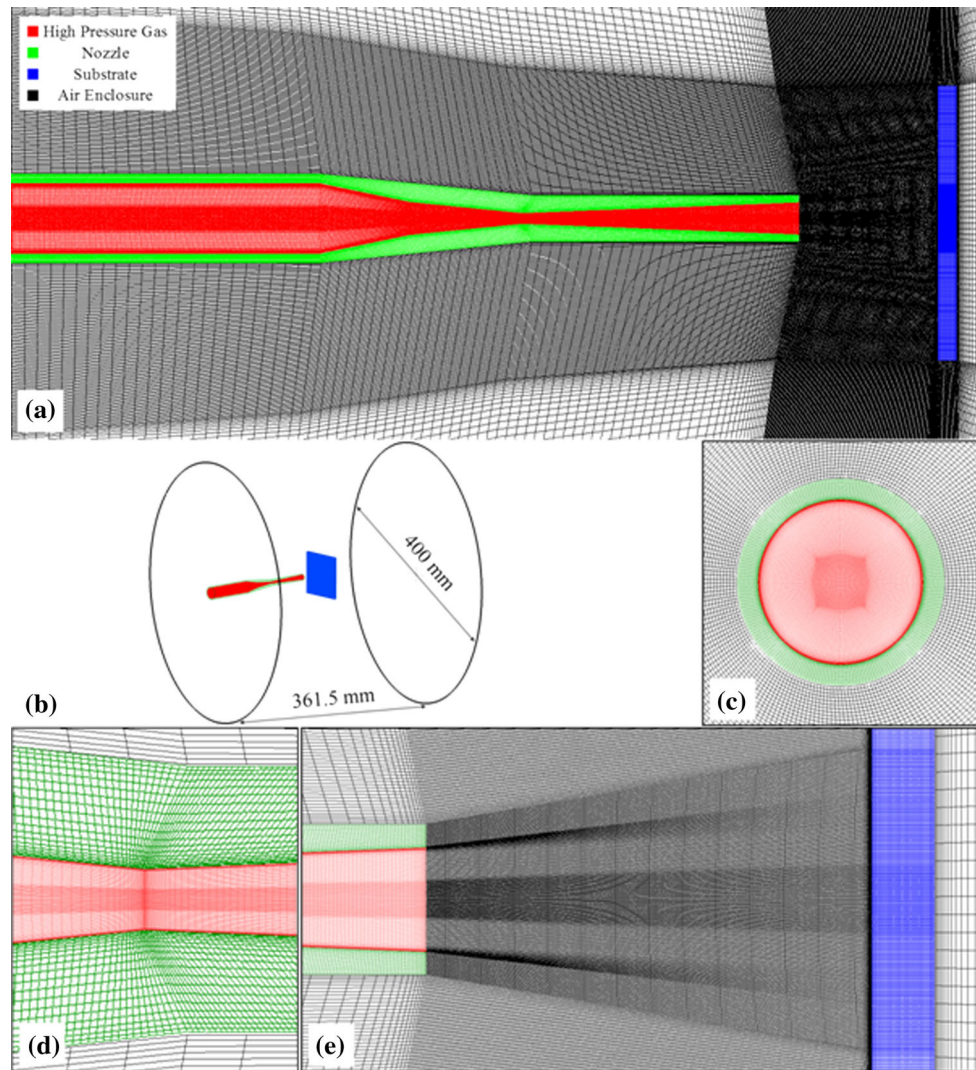
Fig. 1 Developed meshing for fluid and solid domains (a) CFD computational grid, (b) surrounding domain, (c) high pressure gas pre-chamber plane, (d) cold spray nozzle throat and (e) cold spray nozzle exit and substrate surface

The inlet turbulence quantities, k and ε were calculated based on default inlet turbulence intensity ($I = u/U = 0.037$), which was an approximate value for internal cylinder flow, and auto-compute length scale:

$$k_{\text{inlet}} = \frac{3}{2} I^2 U^2, \tag{Eq 13}$$

$$\varepsilon_{\text{inlet}} = \rho C_\mu \frac{k^2}{\mu_t} = \rho C_\mu \frac{k^2}{1000 I \mu}. \tag{Eq 14}$$

The total temperature T_{tot} was also specified at the inlet. The inlet energy flow by diffusion was assumed to be negligible compared to advection and equated to zero. The static temperature T_{stat} was then dynamically computed from the definition of total temperature.

$$T_{\text{stat}} = T_{\text{tot}} - \frac{U^2}{2c_{\text{p}}}. \tag{Eq 15}$$

Opening boundary conditions were set for all domain surrounding surfaces. This specific boundary condition had an advantage over outlet boundary condition because it allowed the gas to cross boundary surfaces in either direction. The interaction between gas and solid walls was assumed as frictionless, which was equivalent to free slip wall boundary condition. In this case, the velocity component parallel to the wall was computed and had a finite value, but the velocity normal to the wall, and the wall shear stress, were both set to zero.

The adiabatic wall boundary condition was set for nozzle pre-chamber inlet plane to prevent heat transfer across the wall boundary. The mechanical and thermal properties of nozzle and substrate were assumed to be isotropic. Second-order accurate approximations were used for discretization of the governing equations, high-resolution scheme was used for advection term calculation, and shape functions were used to evaluate spatial derivatives for all the diffusion terms. The prediction of diffusion terms using shape functions improves solution robustness with negligible local reduction in accuracy of the discrete approximation.
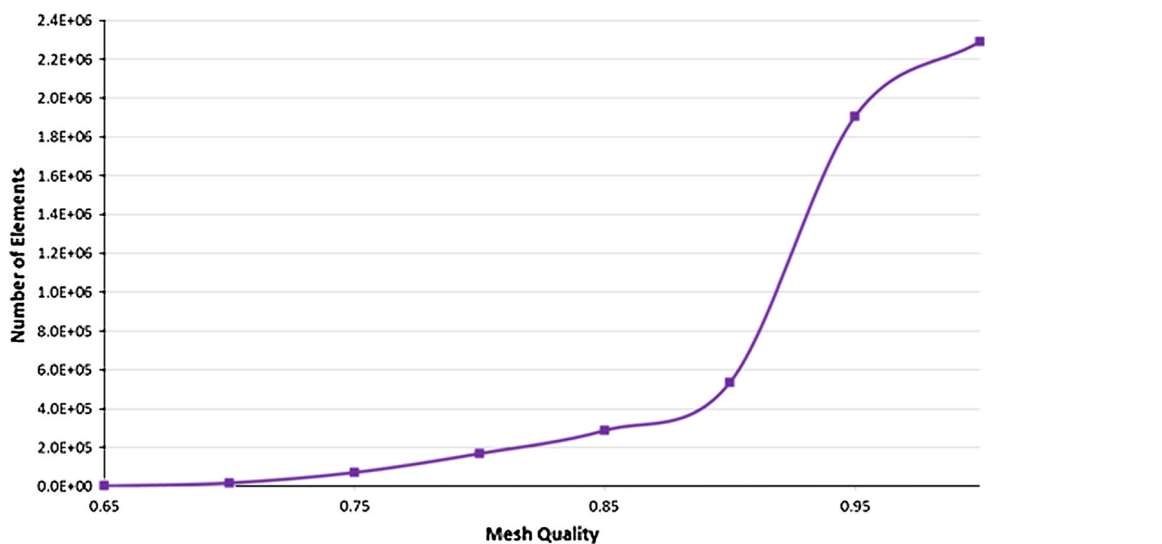
Fig. 2 The average mesh quality for all domains as a function of elements number

It is worth noting that a thin nano-meter naturally formed oxide layer was expected to be present on the surface of titanium substrate which was considered to be insignificant for 3D modeling of this study due to its considerably small thickness.

2.4 Domain Meshing

ANSYS™ ICEMCFD® v14.0 with blocking method was used to create acceptable structured meshes with hexahedral elements for all fluid and solid domains to provide improved convergence. Generally smaller element size improves accuracy of the model predictions with associated compromise for computation time (Ref 30). The transition of meshing between fluids and solid domains is generally set at minimum as large variation at the interface may disturb the convergence. Knowing this, a fine mesh structure was considered for critical locations where large parameter variations were expected. These locations were in the cold spray nozzle throat area, Fig. 1d, jet expansion zone at the nozzle exit and the jet impingement zone in front of the substrate, Fig. 1e. Element size of 0.0225 mm was found to be adequate for throat region to accommodate for sudden change in gas compressive-expansion conditions. To accommodate for rapid change in temperature and velocity, meshing at jet impingement location onto the substrate also had a small element size of 0.1354 mm.

To control the transition between near wall and free-stream turbulence models, inflation layers with $y+$ of about 11 was used at near wall boundaries (Ref 12, 31), particularly at the substrate front surface, Fig. 1a. It was found that smaller $y+$ values increased computation time dramatically without significant improvement in estimation. The mesh size in other zones was considered coarser to optimize the number of elements and improve computation time with the largest element size of approximately 14.1025 mm. Using this approach, a good mesh

quality above 0.6180 was achieved as shown in Fig. 2 with acceptable minimum angle between 38.1° and 89.9°.

3. Experimental Procedure

A KINETIKS® 4000 (Sulzer Metco, Zürcherstrasse, Winterthur, Switzerland) commercial cold spray system was used to achieve supersonic jet. The cold spray nozzle geometries were 51.2-mm converging section, 2.7-mm throat diameter, 70.3-mm diverging section and 8.3-mm exit diameter. The nozzle was made of tungsten carbide (WC) and held normal to the substrate surface using an ABB IRB 2600 robot (ABB Ltd., Affolternstrasse, Zurich, Switzerland). Schematic of cold spray system for experiments of this study is shown in Fig. 3. Supersonic flow was achieved through compression of the gas at the nozzle throat followed by rapid expansion to atmospheric pressure.

A Grade 2 commercial purity (CP) titanium flat plate with $70 \times 70 \times 5 \text{mm}^3$ dimensions was chosen as a substrate. Substrate distance from nozzle exit known as standoff was 35 mm. Titanium was chosen as substrate due to interests in cold spray industrial applications and high temperature integrity for conditions used in this study. Cold spray jet at 550 °C and 1.4 MPa, Table 1, was used for calibration of the 3D CFD model. The developed 3D model was evaluated with respect to experimental temperature measurements at 800 °C and 3 MPa cold spray conditions.

In order to measure temperature, 5 K-type thermocouples were located inside the substrate by machining five holes of 1-mm diameter and 4-mm depth in the substrate rear surface as shown in Fig. 4a. Thermocouples were orientated diagonally on the substrate with 10 mm gap between adjacent thermocouples, Fig. 4b. The cold spray nozzle was aligned as close as possible to the center of the
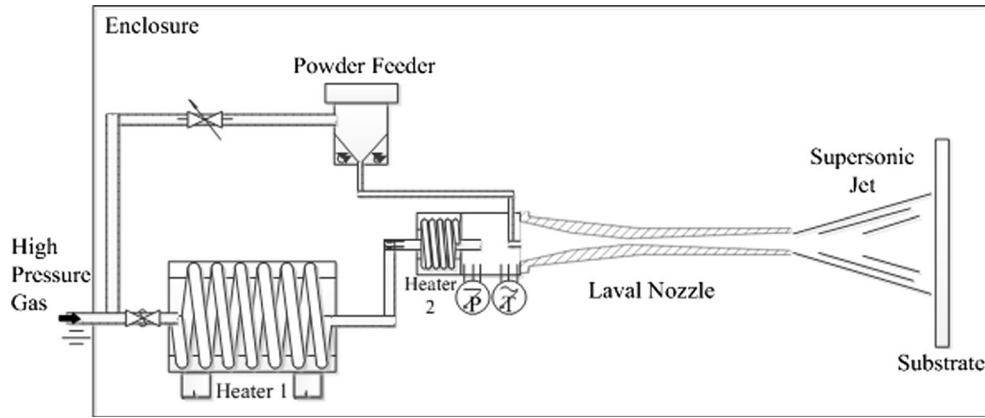
Fig. 3 Schematic diagram of cold spray system used for calibration and experimental evaluation of 3D CFD model

Table 1 Cold spray conditions used for calibration and evaluation of the developed 3D model

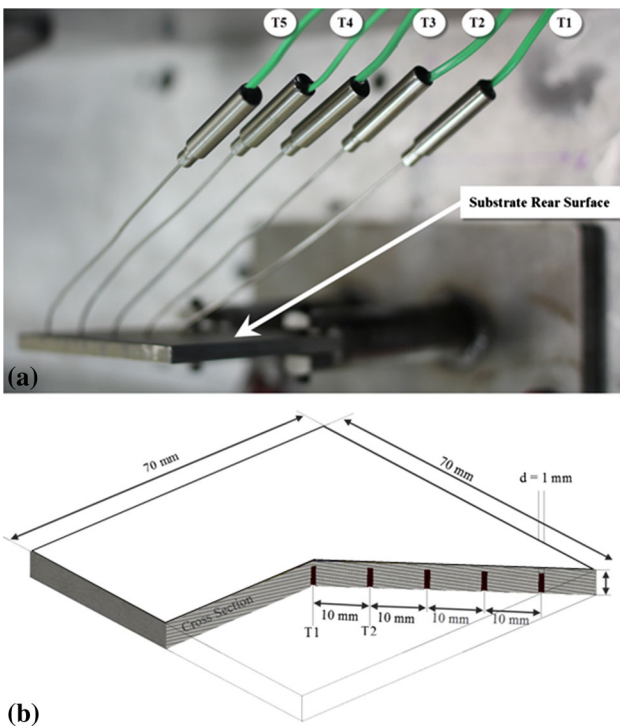| Cold spray condition	Temperature,°C	Pressure, MPa	Standoff, mm
1	550	1.4	35
2	800	3.0	35

Fig. 4 (a) Thermocouples set up attached to rear surface of substrate; and (b) cross section of titanium substrate with thermocouples position oriented diagonally with respect to the center of the specimen

substrate before initiation of the experiment. Temperature measurements were performed using a Pico® data logger with a step size of 1 millisecond. Two sets of temperature measurements were conducted for cold spray conditions shown in Table 1. All thermocouples were calibrated with

±0.5 °C accuracy. Substrate was exposed to cold spray supersonic jet through robot moving the nozzle to its position in front of substrate. Nozzle was rapidly moved away after substrate temperature reached steady state.

3.1 Determination of Jet Center Coordinates on Substrate Surface

Visual inspection of the substrate surface revealed that center of supersonic jet did not exactly impinge onto the center of substrate where T1 was located. This meant that location of jet center on substrate surface had to be determined for development of the heat transfer model. Further to this, it was important to establish a robust calibration process independent of cold spray jet positioned exactly at the center of the substrate eliminating requirements for time consuming and costly high precision jet alignment.

Figure 5 details the approach to determine the location of T1′ a symmetrical point that has identical temperature with T1 on the diagonal line of thermocouples. T1′ position was determined where X1 and X2 in Fig. 5 were equal with respect to peak point M on a parabolic curve that includes T1, T1′, and T2. It is worth noting that parabolic curve was only utilized to assist with simple determination of T1′ location and did not correspond to temperature variations. Position of T1′ at the cross section of circle C1 and the diagonal line of thermocouples is shown in Fig. 6.

T1 and T1′ represent centers of circles C1 and C2, respectively. The intersection of C1 and C2 identified point E that has identical temperature with T1 and T1′. The jet center J was determined as the center of circle C3 that was established from T1, T1′ and E. Using this approach, coordinates of jet center J with respect to substrate center were determined at 4.767 mm and 1.200 mm for X and Y directions, respectively. These coordinates
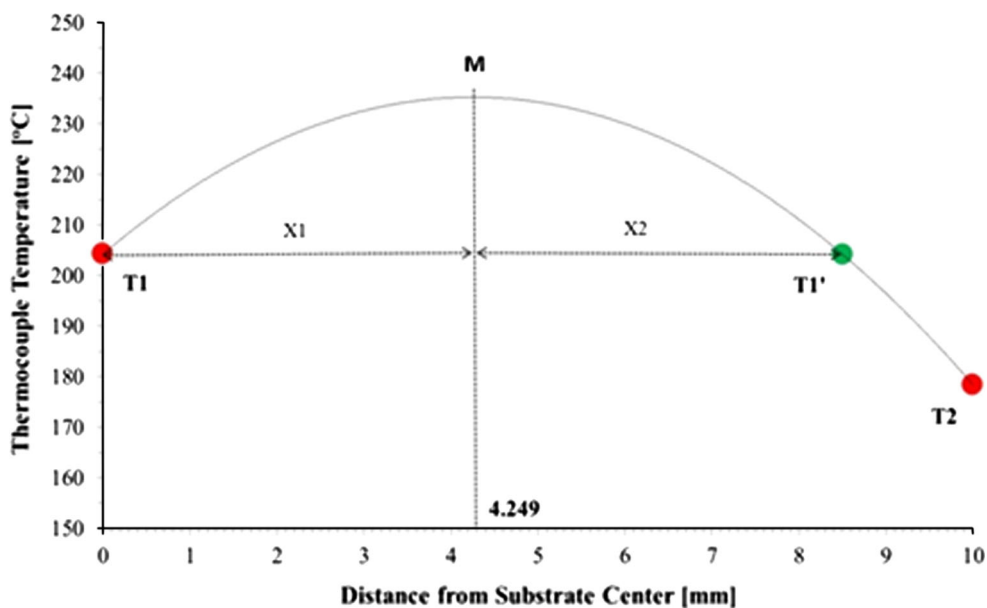
Fig. 5 Determination of T1' location on substrate, with identical temperature as T1, on diagonal line of thermocouples
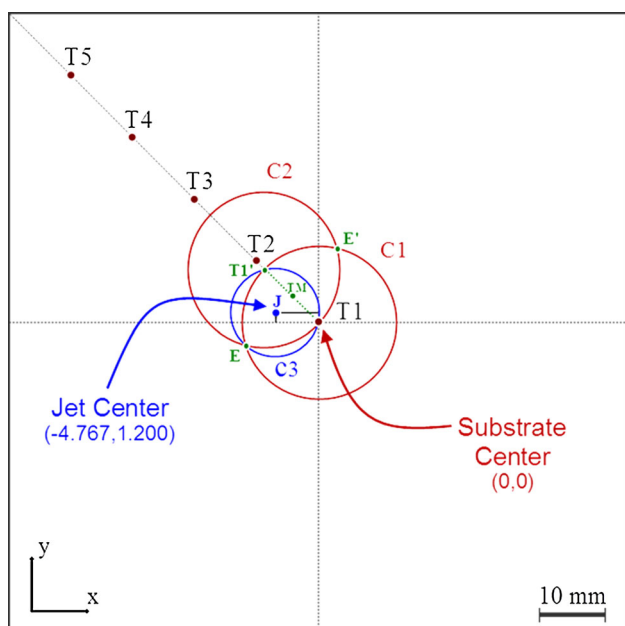

Fig. 6 Measured temperature profiles for five thermocouples attached to CP titanium substrate for cold spray conditions 550 °C and 1.4 MPa

were very closely matched with slight heat-colored circle appeared on substrate surface which was created from impinging cold spray jet.

It is worth noting that cross section of C1 and C2 (E′) in Fig. 6 can provide a second jet center on the opposite direction which provides similar results due to symmetrical nature of the jet center positioning. This approach to identify the cold spray jet center on substrate can be applied to any location close to center of a square

substrate where jet center is positioned between two thermocouples with diagonal arrangement.

4. Results

Figure 7 shows the results of substrate temperature measurements for cold spray condition 1 for all thermocouples. Coordinates of each thermocouple with respect to jet center and corresponding steady-state temperature are reported in Table 2. Thermocouple T1 with the closest location to the jet center reached the highest temperature 204 °C amongst other thermocouples. These results, as expected, presented higher substrate temperatures compared with a recent investigation by Ryabinin et al's (Ref 14) due to considerably higher, 550 °C, cold spray nitrogen stagnation temperature. Similarly, McDonald et al. (Ref 32) infrared temperature measurements of a steel substrate for cold spray conditions of 100 °C stagnation temperature, 0.6 MPa pressure and 10-mm standoff distance revealed maximum substrate temperature 60 °C at the supersonic jet center. In their study, McDonald et al. (Ref 32) proposed a nondimensionalized temperature parameter, θ, as

$$\theta = \frac{T_{\mathrm{w}} - T_{\infty}}{T_{\mathrm{g}} - T_{\infty}}, \tag{Eq 16}$$

where T_{g} is cold spray gas temperature, T_{w} is the measured substrate surface temperature, and T_{∞} is the ambient temperature (for this study 15 °C). The value for θ with respect to the closest thermocouple to the jet center, T1, was 0.35. This was slightly less than McDonald et al. (Ref 32) estimations most likely due to the fact that T1 was not exactly positioned on the jet center.

It took 30 s for thermocouple T1 to reach steady-state temperature (Fig. 7). The maximum temperatures for T2, T3, T4, and T5 thermocouples were 178, 96, 83, and 76 °C, respectively. The largest temperature variation of ±1.5 °C under steady-state condition was recorded for T1 which was considered insignificant for calibration of the 3D model.

4.1 Calibration of the Holistic 3D Model

Calibration of the 3D model was carried out for cold spray nitrogen at 550 °C and 1.4 MPa impinging onto substrate surface at 35-mm standoff. Grade 2 commercial purity titanium properties were chosen for simulation of substrate (Ref 33). An initial domain temperature T_{dom} of 15 °C was used which was similar to cold spray laboratory temperature when experiments were conducted.

The value of environment relative pressure $p_{dom} = 1[atm]$ was held constant over the entire open boundary surfaces, and the direction was taken to be normal to the boundary plane. A user-defined time step function t_{step} based on a generic step function $f(x) = [1 + tanh(kx)]/2$, (Ref 33), was applied instead of automatic

time scale calculation to smoothly control the rapid changes in gas conditions at early stages of computation. The function was recomputed at the end of each time step in order to have a new value for the next step according to Eq 16.

$$t_{step} = t_{stepMIN} \frac{1 + tanh[\alpha_{Min}(atstep - \beta_{Min})]}{2} + t_{stepMAX} \frac{1 + tanh[\alpha_{Max}(atstep - \beta_{Max})]}{2}, \quad (Eq~17)$$

where atstep was accumulated simulation time step, $t_{stepMIN}$ was minimum time step value, $t_{stepMAX}$ was maximum time step value, α was slope characteristic, and β was the slope position.

It was found that Prandtl number 0.3 provides the lowest error with respect to experimental results which was less than the recommended value of 0.9 and 0.5, (Ref 12), reported in earlier literature. The calibrated Prandtl number allowed for improved heat transfer in the gas domain. Table 3 shows a summary of parameters determined for calibration process. All pressure specifications in the model were relative to the reference pressure
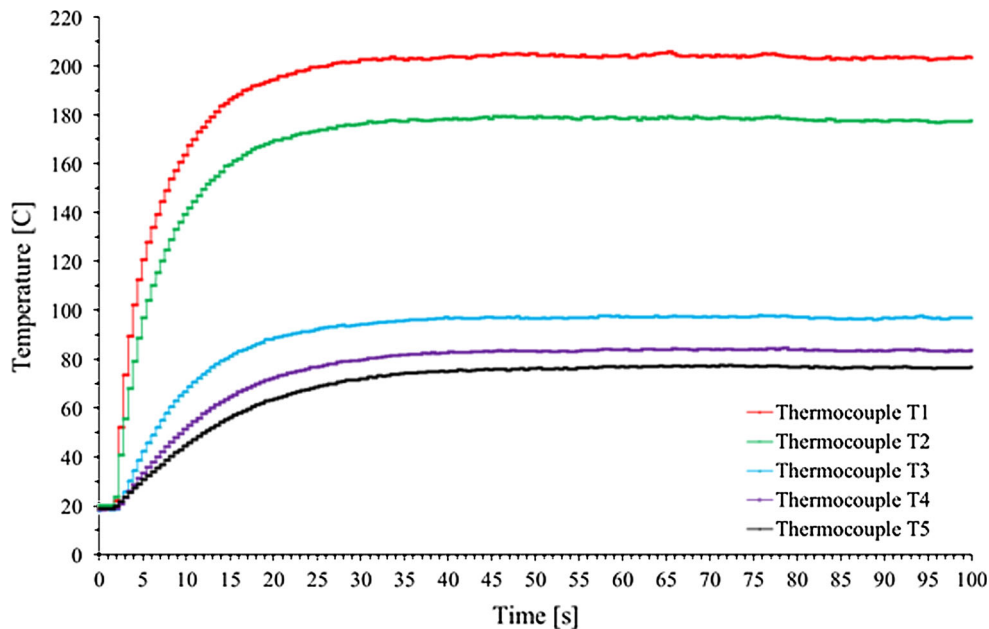

Fig. 7 Diagram representing the method used to determine cold spray supersonic jet center on substrate with respect to experimental results

Table 2 Coordinate of thermocouples with respect to jet center and measured temperature for each thermocouple corresponding to cold spray condition 1

Thermal couple name	X, mm	Y, mm	Distance from substrate center, mm	Distance from jet center, mm	Measured temperature		
					Average, C	Minimum, C	Maximum, C
T1	−4.767	−1.200	0.00	4.92	204.24	202.88	205.74
T2	2.304	5.871	10.00	6.31	178.42	177.26	179.21
T3	9.375	12.942	20.00	15.98	96.87	96.25	97.54
T4	16.446	20.013	30.00	25.90	83.75	83.08	84.65
T5	23.517	27.084	40.00	35.87	76.44	75.24	77.33

Table 3 Original and calibration constants for 3D k-ε model

k-ε model	Pr	$C_{\varepsilon 1}$	$C_{\varepsilon 2}$	C_{Scale}	C_{Clip}
Original	0.90	1.44	1.92	1.00	30.00
Calibrated	0.30	1.65	2.30	10.00	Kato Launder (KL)
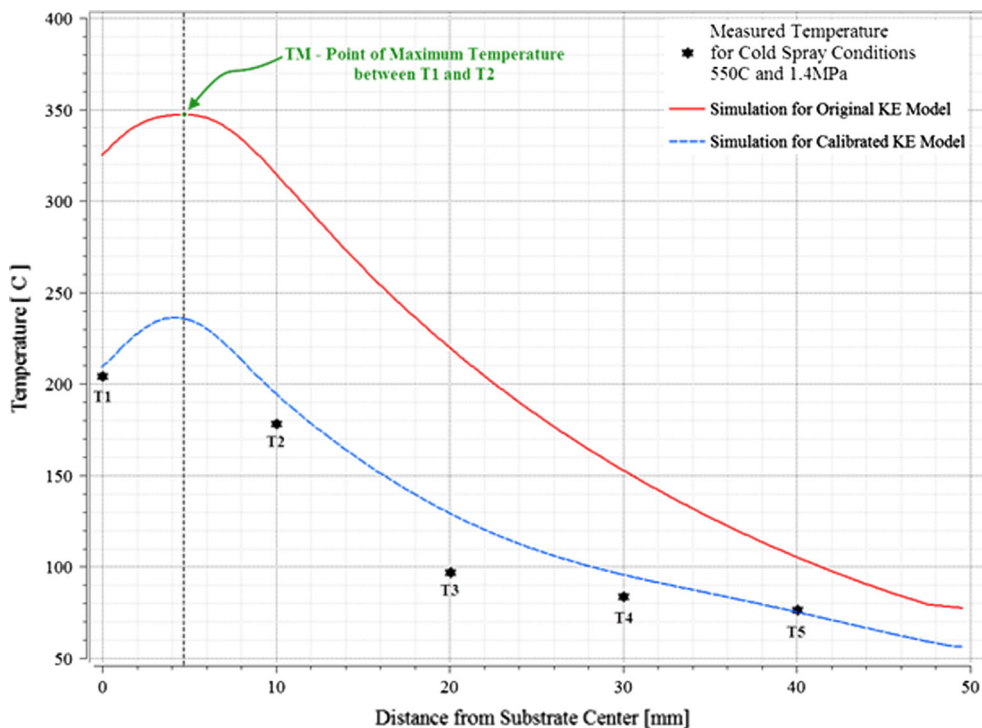
Fig. 8 Comparison of experimental results with original and calibrated 3D models estimations for all thermocouples at 550 °C and 1.4 MPa cold spray conditions
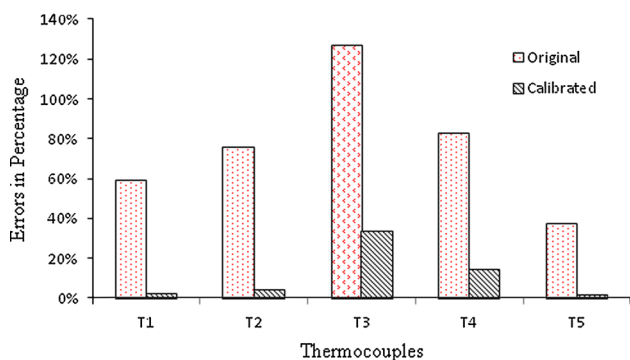
Fig. 9 Original and calibrated 3D model errors for cold spray condition 1

$P_{\text{ref}} = 0$ bar. It was also noted that time steps below 2×10^{-6} s were optimized to achieve robust simulation outcomes.

Figure 8 shows simulated temperatures from original and calibrated k-ε model for cold spray condition 1 compared with measured temperatures. Significant over estimation of substrate temperature from original k-ε model

with respect to experimental results was observed. For instance, temperature of T1 204 °C was over estimated by 59% at 325 °C when original k-ε model was used. This for T2, T3, T4, and T5 was 76, 127, 83, and 38%, respectively.

The estimated temperatures for calibrated model in Fig. 9 represent significantly smaller error with respect to measured temperatures. The computed values for T1 (210) and T2 (195 °C) had very good agreement with measured values 204 and 178 °C, respectively. The error for the original (127%) and calibrated (34%) temperatures for thermocouple 3 was the largest amongst other thermocouples. This was most likely due to a sudden variation in gas condition in the area where T3 was located which require further study. Thermocouple 5 had the lowest 2% calibration error for estimation of temperature which was most likely because of considerable decline in turbulence away from the jet center. The average error for all thermocouples of the calibrated model was 11% which was a considerable improvement compared with 77% for the 3D model with original constants, Table 3.

Figure 10 shows estimated temperatures for calibrated 3D model which includes nozzle, nitrogen from inlet to the titanium surface, and substrate temperature for cold spray
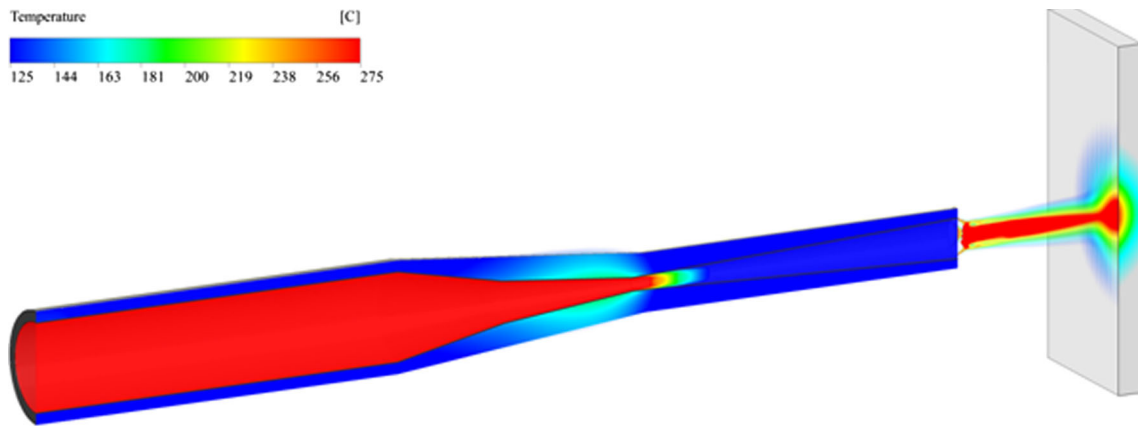
Fig. 10 Estimated temperature for cold spray conditions 550 °C and 1.4 MPa, presented holistically from the gas injection point to the substrate surface, using calibrated 3D model
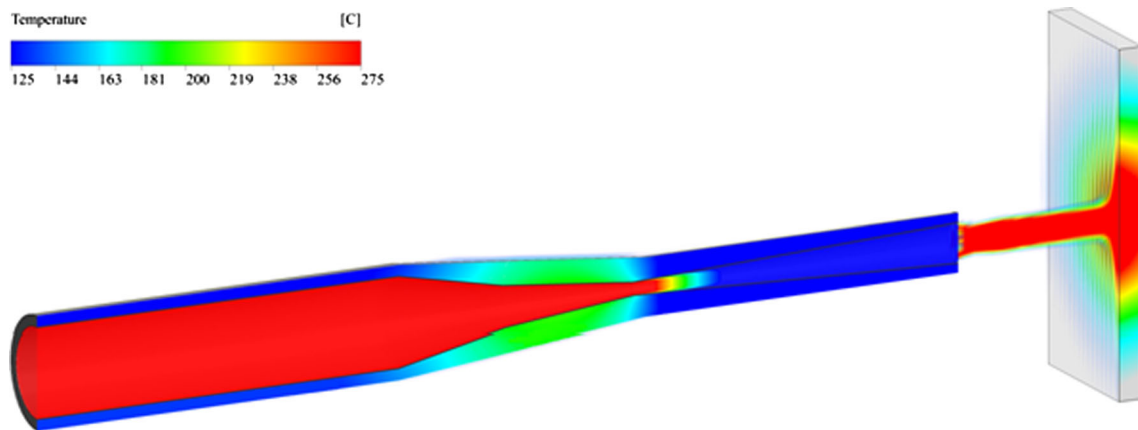

Fig. 11 Estimated temperature for cold spray conditions 550 °C and 1.4 MPa, presented holistically from the gas injection point to the substrate surface, using original k-ε model coefficients

condition 1. The model predicts location of the critical zone for sudden decrease in gas temperature after nozzle throat. The maximum temperature 265 °C was estimated at the jet center on substrate that corresponded to 285 °C decrease from inlet gas temperature 550 °C. The value for θ was 0.47 with respect to the maximum substrate temperature 265 °C for cold spray condition 1. This had a good agreement with McDonald et al. (Ref 32) findings despite their smaller standoff distance 10 mm compared with 35 mm in this study. This was interesting as it was speculated that an increase in standoff could result in a decrease in substrate maximum temperature and θ due to an increase in jet heat loss to environment. It seems that such decrease in θ could be observed at considerably larger standoffs which could be subject of future investigations.

The 3D model estimated temperature distribution on the surface and cross section of substrate (Fig. 10). Similar to cold spray condition 1, the k-ε model with original coefficients, Table 3, considerably overestimated jet temperature as shown in Fig. 11 with maximum substrate temperature 382 °C. The temperature scale for Fig. 11 was

chosen exactly the same as Fig. 10 for easier comparison. These results confirmed that calibration of the holistic 3D model was paramount for achievement of realistic estimations for downstream jet conditions.

5. Evaluation of the Model and Discussion

To be able to validate the calibrated k-ε model, cold spray parameters at considerably higher temperature 800 °C and pressure 3 MPa were chosen (Table 1). The predicted temperatures in Fig. 12 presented a good agreement with experimental results for all thermocouples. The calibrated model outcomes were again significantly better than estimations of k-ε model with original constants shown in Table 3. Further to this, Fig. 13 shows that simulated temperatures for 5 thermocouples had negligible variations in error for cold spray condition 2 compared with cold spray condition 1 with similar total average error of 11% for all thermocouples. Estimated T3
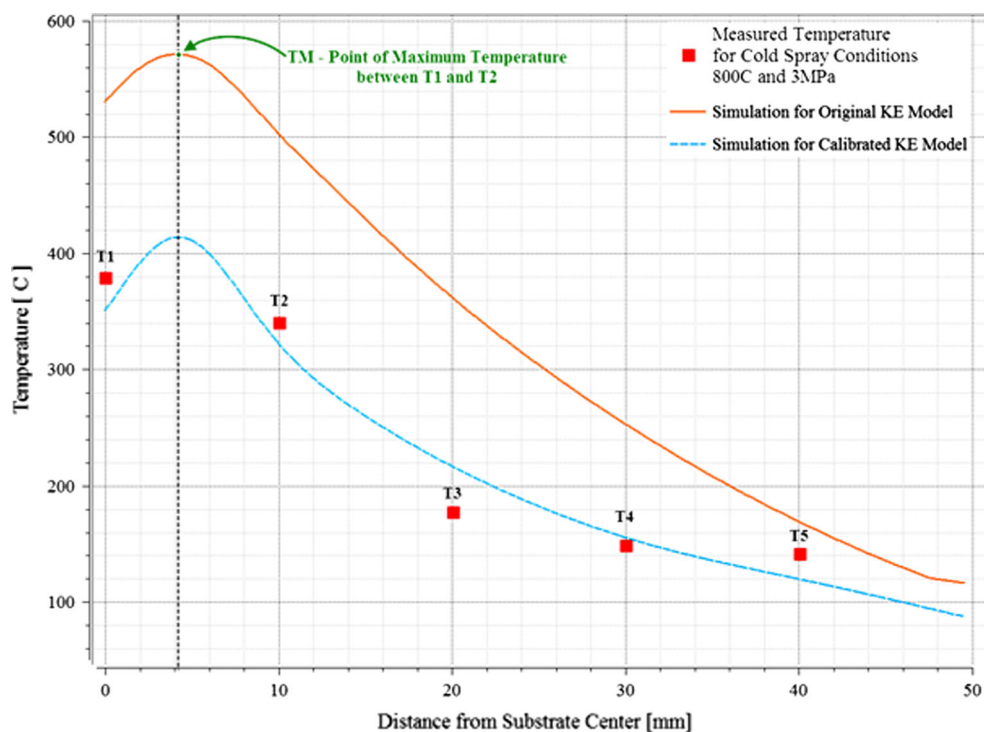
Fig. 12 Estimated temperatures for cold spray conditions 800 °C and 3 MPa compared with original k-ε model and experimental results corresponding to all thermocouples
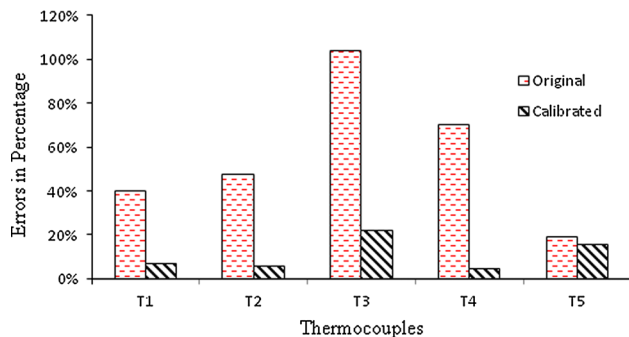

Fig. 13 The developed 3D model errors with respect to experimental temperature measurements for cold spray condition 2 compared with errors corresponding to original k-ε model estimations

presented the highest 22% difference with experimental results for cold spray condition 2 which require further study.

The holistic estimation of temperature for cold spray condition 2 in Fig. 14 revealed thermal events in 4 distinct zones which included the nozzle body, gas phase within the nozzle, supersonic jet outside of nozzle, and temperature profile within substrate. The estimated maximum temperature 410 °C at the jet center impinging onto the substrate was almost half of the inlet gas temperature. Considering earlier investigations by Fukumoto et al. (Ref 7), under this condition a significant improvement in deposition efficiency is expected due to higher substrate temperature. The value for θ with respect to maximum

temperature estimated on substrate surface was 0.5 which was again in good agreement with McDonald et al. (Ref 32) investigations. A similar value 0.5 was estimated for θ with respect to experimental results achieved by Yin et al. (Ref 11) for an Aluminum substrate exposed to cold spray jet at 400 °C, 2.7 MPa and 30-mm standoff distance.

Further to this, for conditions of this study, the model estimated that a 250 °C increase in inlet gas temperature contributes to 145 °C increase in maximum temperature on substrate surface (Fig. 10, 14). This could be due to the heat loss through the nozzle wall and the jet between nozzle exit and substrate surface. These model predictions suggest that any cooling process that leads to a decrease in nozzle body temperature could result in a decrease in maximum temperature achieved on substrate. According to Fukumoto et al. (Ref 7) this could have implications for cold spray bond formation and properties of the deposited material.

A tangible example for holistic model application for design of cold spray system could be the cooling systems design for cold spray nozzle. A general practice for some of the current cold spray system designers and manufacturers is to cool the whole nozzle body using water or gas. This is to achieve certain conditions, i.e., to prevent blockage of nozzle at the throat when certain particles used. The model suggests that cooling the stagnation zone before throat could only result in loss of energy with negligible benefits to deposition process. Further to this, it seems that cooling the areas close to the nozzle exit is not beneficial due to achievement of low temperature from rapid gas expansion. The model simulations, however,
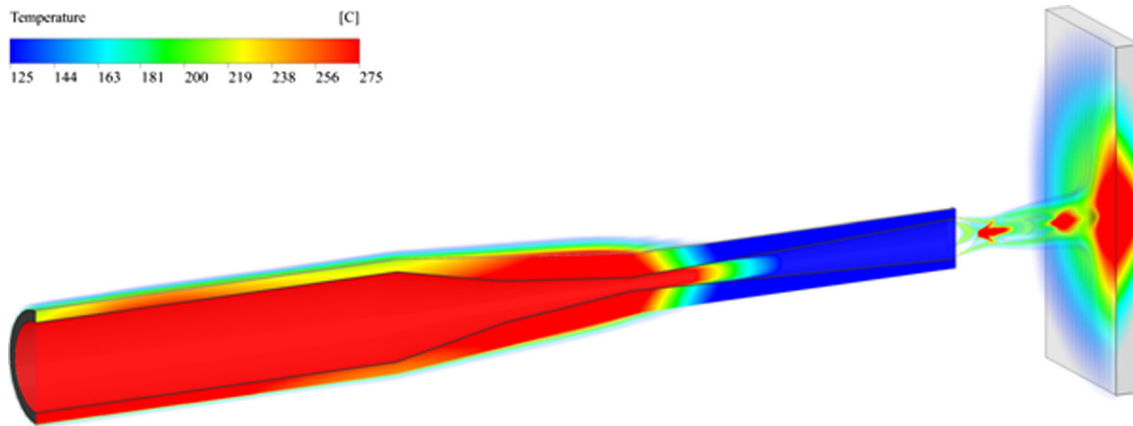
Fig. 14 3D simulation of temperature distribution for cold spray supersonic nitrogen at 800 °C and 3 MPa presented holistically from the nozzle stagnation zone to the substrate surface
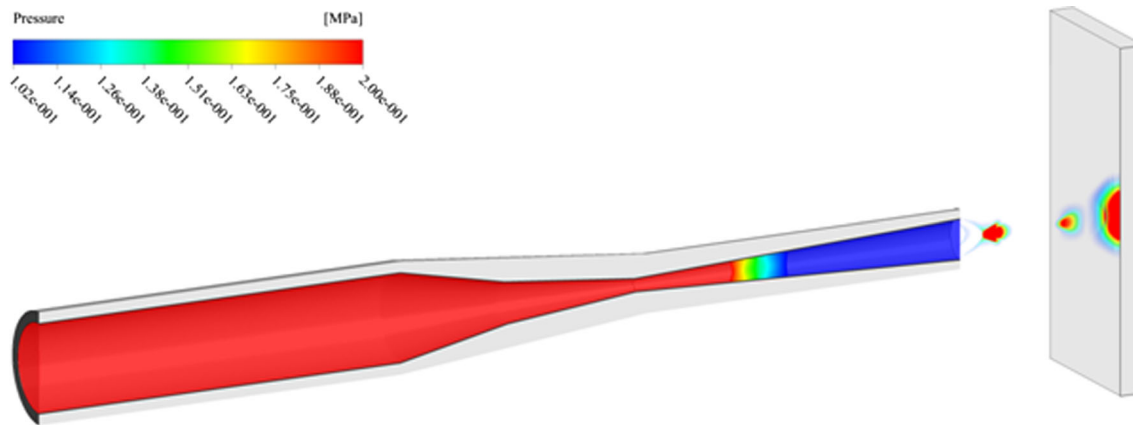

Fig. 15 3D simulation of gas pressure for cold spray conditions 800 °C and 3 MPa presented holistically from gas injection point to the surface of substrate

indicate that perhaps a carefully chosen small zone close to cold spray nozzle throat could provide the optimized local cooling for certain applications. Investigation of cold spray system design is not subject of this study; however, it seems the holistic 3D model could provide a cost-effective approach to improve energy efficiency of current cold spray systems.

The model predictions quantified inhomogeneous distribution of temperature in cold spray nozzle body including a high temperature zone around nozzle throat in agreement with Li et al. studies (Ref 10). Figure 14 shows that thermal events for the gas inside the nozzle were different from the nozzle body. A distinct area at the vicinity of the nozzle throat with significant, 150 °C, variations in nozzle body temperature was predicted. A similar sudden variation of gas temperature occurred within the nozzle that extended further away from the nozzle throat. This zone was larger than similar gas temperature profile for cold spray condition 1 in Fig. 10.

Simulation estimated a diamond-shape high temperature zone with maximum 749 °C between the nozzle exit and the substrate. A complicated, dome shape, 3D

temperature profile on substrate surface was predicted, Fig. 14. The highest surface temperature estimated for this zone was 410 °C at the jet center that was of particular interest due to thermal effects on cold spray particles and bond formation under deposition conditions. Temperature profile within substrate was similar to earlier observations (Ref 10, 11, 14, 32) presenting a decline away from the impinging jet with the lowest temperature 36 °C at the corners of substrate. The holistic model simulations for gas pressure predicted the size and position of diamond shocks within the supersonic jet and bow shock on the substrate, Fig. 15.

The holistic model computations for gas velocity from the inlet to the substrate surface are presented in Fig. 16. The highest velocity at the nozzle exit was estimated 1310 m/s which had a very good agreement with one-dimensional models prediction 1303 m/s. Details of one-dimensional model for estimation of gas velocity can be found elsewhere (Ref 34). A significant increase in nitrogen turbulence kinetic energy on substrate was predicted as shown in Fig. 17. For example, turbulence kinetic energy at the nozzle exit was 11 m²/s² which increased
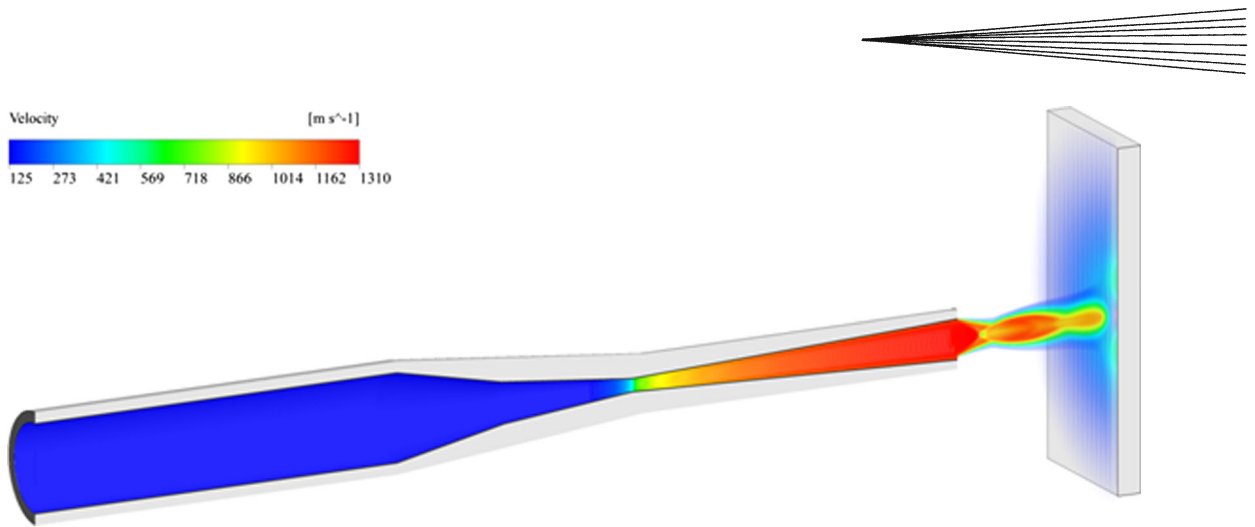
Fig. 16 3D simulation of gas velocity for cold spray conditions 800 °C and 3 MPa presented holistically from nozzle stagnation area to the surface of substrate
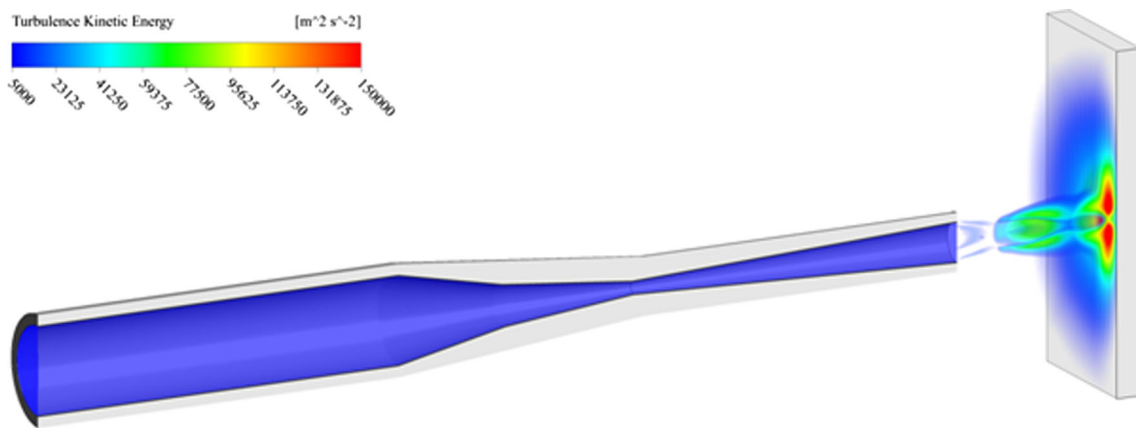

Fig. 17 3D simulation of turbulent kinetic energy for cold spray conditions 800 °C and 3 MPa demonstrated holistically from nozzle stagnation zone to the substrate surface
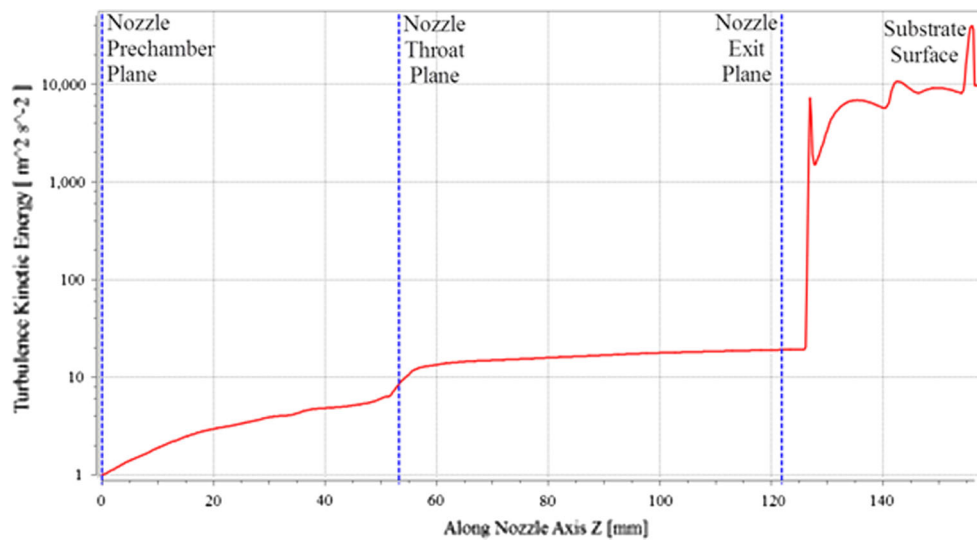

Fig. 18 Computed turbulence kinetic energy with respect to nozzle axis for cold spray nitrogen at 800 °C and 3 MPa

almost 4 orders to 40,000 m^2/s^2 further away from the nozzle exit (Fig. 18). This is interesting due to the potential to quantify the impact of substrate and nozzle distance (standoff) on downstream cold spray supersonic jet which is crucial for optimization of the deposition process. For instance, Fig. 18 shows that 35-mm standoff was optimized allowing high turbulence to occur further away from the nozzle exit avoiding disruption of supersonic gas flow up stream inside the nozzle. A useful investigation for future could be to utilize the holistic model to quantify the effect of high turbulence zone in Fig. 17 and 18 on position, velocity, and temperature of supersonic particles inside the cold spray plume. This could provide a complete history of the particles just before impact and through bond formation in the deposition zone that is very difficult to achieve through experimentation.

The model simulations particularly have provided opportunities for further fundamental studies in 3D heat transfer modeling of round supersonic jet. For instance, calibration results revealed considerable effect of original Pt number in over estimation of temperature for conditions of this study. The reason for this is not well understood, however, it seems that cold spray jet turbulent thermal conductivity, λ_t, was more dominant than turbulent viscosity μ_t. This means that there is a strong tendency for conduction and away from convection for cold spray supersonic jet. It is worth highlighting that complicated nature of cold spray supersonic jet demands for further development and examination of the 3D model estimations. For instance, comparison of the model outcomes with other CFD modeling approaches such as V^2-F could be beneficial.

In terms of practical applications for cold spray industry, this study aimed to provide the early steps for demonstration of advanced 3D models that could eventually simulate complicated scenarios in cold spray deposition by tracking gas and particle from inlet to the substrate surface. This was with the emphasis on the fact that only a validated model for cold spray gas can provide realistic and reliable information for history of cold spray particles in the deposition zone. This is paramount for optimization of cold spray unique nano-second bond formation and improvement of deposited material properties. It is speculated that such advanced 3D models will assist industry to improve cold spray systems in addition to the development of novel additive manufacturing processes based on fundamentals of this unique solid-state deposition technology.

6. Conclusions

A holistic 3D model was successfully developed to simultaneously estimate state of all cold spray system components including nozzle, substrate, and supersonic jet. A broadly utilized k-ε-type model was calibrated and validated with respect to measured temperature for a titanium substrate exposed to cold spray jet. The 3D model revealed a detailed snapshot of complicated events with respect to cold spray gas velocity, temperature, pressure, and turbulence from the point of gas injection to the location at which supersonic jet impinges onto the substrate. The model estimations for cold spray jet could be utilized to achieve realistic 3D approximations for state of individual cold spray particles from the injection point to the deposition zone. The model was developed with consideration of users in industry with limited access to supercomputers.

References

1. A. Papyrin, V. Kosarev, S. Klinkov, A. Alkhimov, and V.M. Fomin, *Cold Spray Technology*, 1st edn., Elsevier, 2007, p 14-20
2. S.H. Zahiri, W. Yang, and M. Jahedi, Characterization of Cold Spray Titanium Supersonic Jet, *J. Therm. Spray Technol.*, 2009, **18**(1), p 110-117
3. M. Fukumoto, M. Mashiko, M. Yamada, and E. Yamaguchi, Deposition Behavior of Copper Fine Particles onto Flat Substrate Surface in Cold Spraying, *J. Therm. Spray Technol.*, 2010, **19**(1–2), p 89-94
4. H. Katanoda, M. Fukuhara, and N. Iino, Numerical Study of Combination Parameters for Particle Impact Velocity and Temperature in Cold Spray, *J. Therm. Spray Technol.*, 2007, **16**(5-6), p 627-633
5. P.C. King and M. Jahedi, Relationship Between Particle Size and Deformation in the Cold Spray Process, *Appl. Surf. Sci.*, 2010, **256**(6), p 1735-1738
6. C.J. Li and W.Y. Li, Deposition Characteristics of Titanium Coating in Cold Spraying, *Surf. Coat. Technol.*, 2003, **167**(2–3), p 278-283
7. M. Fukumoto, H. Wada, K. Tanabe, M. Yamada, E. Yamaguchi, A. Niwa, M. Sugimoto, and M. Izawa, Effect of Substrate Temperature on Deposition Behavior of Copper Particles on Substrate Surfaces in the Cold Spray Process, *J. Therm. Spray Technol.*, 2007, **16**, p 643-650
8. W. Wong, E. Irissou, A. Ryabinin, J.G. Legoux, and S. Yue, Influence of Helium and Nitrogen Gases on the Properties of Cold Gas Dynamic Sprayed Pure Titanium Coatings, *J. Therm. Spray Technol.*, 2010, **20**, p 213-226
9. J.G. Legoux, E. Irissou, and C. Moreau, Effect of Substrate Temperature on the Formation Mechanism of Cold-Sprayed Aluminum, Zinc, and Tin Coatings, *J. Therm. Spray Technol.*, 2007, **16**, p 619-626
10. W. Li, S. Yin, X. Guo, H. Liao, X. Wang, and C. Coddet, An Investigation on Temperature Distribution Within the Substrate and Nozzle Wall in Cold Spraying by Numerical and Experimental Methods, *J. Therm. Spray Technol.*, 2012, **21**, p 41-48
11. S. Yin, X. Wang, W. Li, and X. Guo, Examination on Substrate Preheating Process in Cold Gas Dynamic Spraying, *J. Therm. Spray Technol.*, 2011, **20**(4), p 852-859
12. D.C. Wilcox, *Turbulence Modelling for CFD*, 3rd edn., DCW Industries, La Canada Flintridge CA 91011, 2000
13. S. Yin, W.Y. Li, and Y. Li, Numerical Study on the Effect of Substrate Size on the Supersonic Jet Flow and Temperature Distribution Within the Substrate in Cold Spraying, *J. Therm. Spray Technol.*, 2012, **21**(3-4), p 628-635
14. A. Ryabinin, E. Irissou, A. McDonald, and J.G. Legoux, Simulation of Gas-Substrate Heat Exchange During Cold Gas Dynamic Spraying, *Int. J. Therm. Sci.*, 2012, **56**, p 12-18
15. C. Lee, M. Chung, K. Lim, and Y. Kang, Measurement of Heat Transfer from a Supersonic Impinging Jet onto an Inclined Flat Plate at 45°, *J. Heat Transf.*, 1991, **113**, p 769-772
16. V. Ramanujachari, S. Vijaykant, R. Roy, and P. Ghanegaonkar, Heat Transfer Due to Supersonic Flow Impingement on a Vertical Plate, *Int. J. Heat Mass Transf.*, 2005, **48**, p 3707-3712
17. I. Belov, I. Ginzburg, and L. Shub, Supersonic Underexpanded Jet Impingement Upon Flat Plate, *Int. J. Heat Mass Transf.*, 1973, **16**, p 2067-2076
18. M. Rahimi, I. Owen, and J. Mistry, Impingement Heat Transfer in an Under-Expanded Axisymmetric Air Jet, *Int. J. Heat Mass Transf.*, 2003, **46**, p 263-272
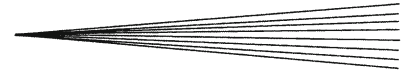
19. T.D. Phan, S.H. Masood, M.Z. Jahedi, and S. Zahiri, Residual Stresses in Cold Spray Process Using Finite Element Analysis, *Mater. Sci. Forum*, 2010, **654-656**, p 1642-1645

20. M. Karimi, A. Fartaj, G. Rankin, D. Vanderzwet, W. Birtch, and J. Villafuerte, Numerical Simulation of the Cold Gas Dynamic Spray Process, *J. Therm. Spray Technol.*, 2006, **15**(4), p 518-523

21. H. Tabbara, S. Gu, D.G. McCartney, T.S. Price, and P.H. Shipway, Study on Process Optimization of Cold Gas Spraying, *J. Therm. Spray Technol.*, 2011, **20**(3), p 608-620

22. W.Y. Li, S. Yin, X. Guo, H. Liao, X.F. Wang, and C. Coddet, An Investigation on Temperature Distribution Within the Substrate and Nozzle Wall in Cold Spraying by Numerical and Experimental Methods, *J. Therm. Spray Technol.*, 2012, **21**(1), p 41-48

23. E. Smith, J. Mi, G. Nathan, and B. Dally, *Preliminary Examination of a Round Jet Initial Conditions Anomaly for k-ε Turbulence Model, 15th Australian Fluid Mechanics Conference*, The University of Sydney, Sydney, Australia, 2004, p 13-17

24. F.R. Menter, Two-equation Eddy-Viscosity Turbulence Models for Engineering Applications, *AIAA J.*, 1994, **32**(8), p 1598-1605

25. F.R. Menter, Eddy-Viscosity Transport Equations and Their Relation to the k-ε Model, *J. Fluids Eng.*, 1997, **119**, p 876-884

26. S. Gu, C.N. Eastwick, K.A. Simmons, and D.G. McCartney, Computational Fluid Dynamic Modeling of Gas Flow Charac-teristics in a High-Velocity Oxy-Fuel Thermal Spray System, *J. Therm. Spray Technol.*, 2000, **10**(3), p 461-469

27. J.E. Bardina, P.G. Huang, and T.J. Coakley, Turbulence Modeling Validation, Testing, and Development, *NASA Tech. Memo.*, 1997, **110446**, p 32-34

28. B.E. Poling, J.M. Prausnitz, and J.P. O'Connell, *The Properties of Gases and Liquids, Vol. 5*, McGraw-Hill, New York, 2001

29. H. Schlichting, *Boundary Layer Theory*, McGraw-Hill, New York, 1979

30. P.R. Spalart, Strategies for Turbulence Modelling and Simulations, *Int. J. Heat Fluid Flow*, 2000, **21**(3), p 252-263

31. H. Grotjans and F.R. Menter, Wall Functions for General Application CFD Codes, In *Proceedings of Fourth European Computational Fluid Dynamics Conference*, Wiley, Athens, 1998, p 1112-1117

32. A. McDonald, A.N. Ryabinin, E. Irissou, and J.G. Legoux, Gas-Substrate Heat Exchange During Cold-Gas Dynamic Spraying, *J. Therm. Spray Technol.*, 2013, **22**, p 391-397

33. R. Boyer, G. Welsch, and E.W. Collings, *Materials Properties Handbook: Titanium Alloys*, 3 edn., ASM Int., The Mat. Inf. Soc., 2003

34. G. Franz, F. Abed-Meraim, J.P. Lorrain, T.B. Zined, X. Lemoine, and M. Berveiller, Ellipticity Loss Analysis for Tangent Moduli Deduced from a Large Strain Elastic-Plastic Self-Consistent Model, *Int. J. Plast.*, 2009, **25**(2), p 205-238